remote sensing

MDPI

Article

Spatiotemporal Analysis of Vegetation Fires and Carbon Monoxide Pollution in Indonesia

Griffin McAvoy [1] and Krishna Vadrevu [2,*]

[1] Atmospheric Science Department, University of Alabama in Huntsville, Huntsville, AL 35899, USA; gtm0006@uah.edu
[2] NASA Marshall Space Flight Center, Huntsville, AL 35899, USA
* Correspondence: krishna.p.vadrevu@nasa.gov

Highlights

What are the main findings?

- In Indonesia, fire activity declined overall between 2012 and 2024 but remained persistent. Strong seasonal peaks continue during the dry season, especially from August to October, with fire activity intensifying by more than 400% during El Niño years.
- Spatial regression revealed that fire activity is closely correlated with carbon monoxide (CO) pollution, particularly in the forested regions of central Kalimantan, western Sulawesi, and southern Java.

What is the implication of the main finding?

- Persistent seasonal peaks and El Niño–driven fire surges highlight the need to integrate fire management into climate adaptation and public health planning.
- Strong spatial links between fires and CO pollution in specific regions suggest that region-focused interventions in forests and peatlands could deliver the greatest benefits for air quality and emission reduction in Indonesia.

Abstract

Vegetation fires in Indonesia, particularly in forests and peatlands, are major drivers of air pollution, with impacts on public health, biodiversity, and climate. Using satellite-derived data from 2012 to 2024, we identified an average of 21,271 fires annually, with peak activity during the dry season (August–October). 32.0% of total fires occurred in forests; and 21.9% in peatlands. While a seasonal Mann–Kendall trend analysis revealed a statistically significant decline in fire activity over this period (approximately 502 fewer fires per month), seasonal peaks remain persistent during the late and post-monsoon periods. Notably, fire activity increased by more than 400% during El Niño years (2015–2016, 2018–2019, 2023–2024) compared to non-El Niño years. Through geographically weighted regression (GWR), we found that fire activity is closely correlated to carbon monoxide (CO) pollution. The relationship was strongest in the forested regions of central Kalimantan, western Sulawesi, and southern Java. Our findings highlight the amplifying effects of El Niño events on fire dynamics and air quality and the urgent need for targeted, climate-responsive fire management strategies. Strengthening mitigation and adaptation efforts in tropical forests and peatlands will be critical for protecting human health and reducing emissions in the region.

Keywords: fires; El Niño; carbon monoxide; forests; peatlands; Indonesia

Academic Editor: Xiaoyang Zhang

Received: 2 July 2025
Revised: 3 September 2025
Accepted: 16 September 2025
Published: 24 September 2025

Citation: McAvoy, G.; Vadrevu, K. Spatiotemporal Analysis of Vegetation Fires and Carbon Monoxide Pollution in Indonesia. *Remote Sens.* **2025**, *17*, 3275. https://doi.org/10.3390/rs17193275

1. Introduction

Vegetation fires are a persistent environmental challenge across Southeast Asian countries, with varying causes and impacts depending on the country [1–3]. While natural fires occur in some ecosystems, human-induced fires are the dominant source of burning in many parts of the continent, where land clearing, agriculture, and shifting land use practices drive fire activity [3–6]. Among Asian countries, Indonesia experiences some of the most severe and frequent wildfires, mainly due to a combination of climatic conditions, land management practices, and anthropogenic activities [7].

Indonesia, the world's largest archipelagic nation, is situated on the equator and consists of over 17,000 islands (Figure 1), making it one of Earth's most geographically diverse countries [8]. The country is predominantly covered by tropical rainforests, which play a critical role in global biodiversity and carbon storage. Indonesia's climate is characterized by high temperatures and humidity year-round, with a distinct wet and dry season [9]. Jakarta, the capital and one of the world's largest megacities, exemplifies the country's urban expansion and growing environmental pressures [10].

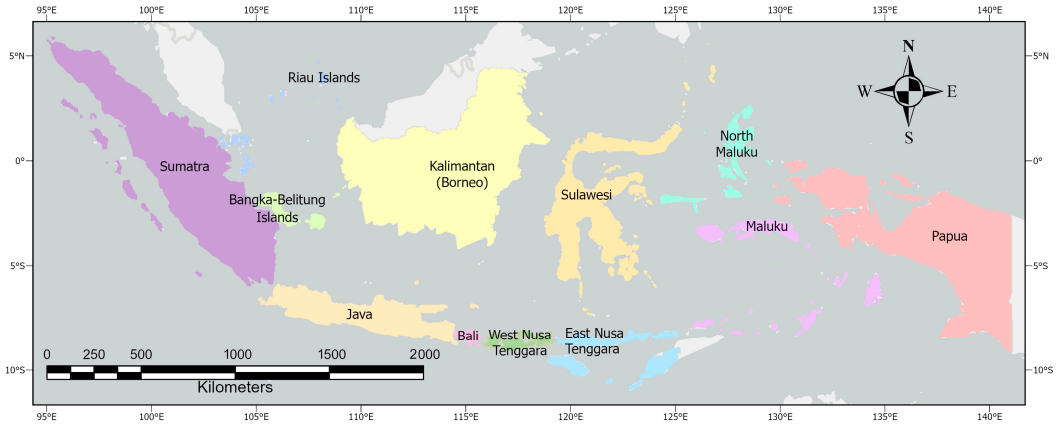

Figure 1. Major regions of Indonesia.

Fires in Indonesia coincide with the dry season, which occurs during the Northern Hemisphere's fall months [11,12]. While some fires are naturally ignited by lightning or underground coal seams, human activities are the primary drivers of vegetation fires in Indonesia [13,14]. Fires are frequently set for agricultural purposes, including land clearing for palm oil plantations and small-scale farming, as well as to facilitate timber extraction and access to forest resources. The risk of fires increases due to land use changes such as logging, road development, and resettlement projects, which alter forest structure, reduce canopy cover, and create drier microclimates conducive to burning [15].

The fire situation is exacerbated during El Niño years, when prolonged drought conditions significantly heighten the fire risks. During El Niño events, rainfall patterns shift eastward, leaving Indonesia drier than usual [16–18]. Based on historical El Niño occurrences from 2012 to 2024, the following years experienced El Niño conditions: (a) 2015–2016: One of the strongest El Niño events, causing severe droughts and extensive peatland fires in Indonesia (b) 2018–2019 A weak-to-moderate El Niño developed in late 2018 and persisted into 2019, influencing drier conditions and fire risks; (c) 2023–2024 (July 2023–May 2024): An El Niño developed in mid-2023, continuing into early 2024, leading to drier-than-normal conditions across Indonesia.

Peatlands, which store vast amounts of carbon, become highly flammable under these El Niño conditions. Fires on drained peatlands are particularly concerning because they burn underground, release massive amounts of carbon monoxide and methane, and persist for months, contributing heavily to air pollution and greenhouse gas emissions [12,19,20].

Fires in Indonesia have profound environmental, economic, and health impacts. The 1997–1998 fire season alone caused damages estimated at nearly $10 billion, burning approximately 4.8 million hectares of forest and agricultural land [21]. The haze from these fires affects Indonesia and neighboring countries such as Malaysia, Singapore, and Thailand, disrupting transportation, reducing air quality, and causing severe public health crises [22]. The 2015 fire season was even more devastating, burning over 2.6 million hectares of land, releasing vast amounts of carbon, and resulting in an estimated economic loss of $16 billion.

The environmental consequences are equally alarming. Wildfires destroy critical habitats for endangered species such as orangutans, tigers, and rhinos [23]. Carbon emissions from Indonesian peatland fires are among the highest globally, with some single day burning events in 2015 emitting more carbon than the entire U.S. economy [24]. In addition to carbon dioxide, wildfires emit large amounts of carbon monoxide (CO), a major pollutant that affects air quality and human health [25]. Unlike industrial combustion processes, which burn fuel more efficiently, vegetation fires burn at lower temperatures and release disproportionately high amounts of CO, methane, and particulate matter. Peatland fires, in particular, release three times as much CO and ten times as much methane as grassland fires, making them a significant contributor to air pollution and global climate change [26]. In general, long-term human exposure to particulate matter can adversely affect public health causing smoke-related respiratory infections including increasing the risk of death [27].

Remote sensing technologies, with their unique characteristics such as multi-spectral, multi-temporal, synoptic, and repetitive capabilities, provide robust information for both fire mapping and monitoring, including pollution episodes. Several studies have employed satellite remote sensing data to characterize fire activity and air pollution in Indonesia, particularly in regions like Sumatra and Kalimantan, where peatland fires are prevalent. MODIS (Moderate Resolution Imaging Spectroradiometer) aboard NASA's Terra and Aqua satellites has been widely used to detect active fires and estimate aerosol optical depth (AOD), revealing the severity of the 2015 fire season [28]. European Space Agency Sentinel data have also been widely applied in fire studies; for example, Sentinel-1 data have been used to characterize Indonesia's 2015 fire-affected areas and estimate carbon emissions [29]. Both mono-temporal and multi-temporal Sentinel-2 satellite data, combined with machine learning algorithms, were employed for burnt area detection in Rokan Hilir Regency, Indonesia [30]. Additionally, a combination of Sentinel-1 and Sentinel-2 data was used for monthly burned-area mapping through multi-sensor integration and machine learning, as demonstrated in a case study of the 2019 fire events in South Sumatra Province [31]. Sentinel-5P's TROPOMI provides data on atmospheric composition, including air pollutants such as NO_2, SO_2, and CO, and has been used to examine spatial-temporal variations in air pollutants across four provinces on Sumatra Island [32]. Himawari-8, a Japanese geostationary satellite, offers high-frequency imagery for monitoring fires and smoke, and studies have demonstrated its capability in detecting fire locations and smoke distribution over Sumatra and Kalimantan during the 2015 fire season [33]. VIIRS (Visible Infrared Imaging Radiometer Suite) aboard NOAA's Suomi NPP and NOAA-20 satellites has been utilized to detect fire hotspots and thermal anomalies [34], including the identification of smoldering peatland fires in Indonesia via triple-phase temperature analysis of VIIRS nighttime data [35]. Collectively, these studies highlight the critical role of satellite remote sensing in monitoring fire activity and air pollution in Indonesia.

Understanding and mitigating Indonesia's wildfire crisis is critical for environmental conservation, climate change mitigation, and public health. Fires not only cause immediate economic losses and habitat destruction but also contribute significantly to long-term at-

mospheric carbon levels. In this study, we focus on vegetation fires and Carbon monoxide pollution in Indonesia. We utilized remote sensing data to address key questions regarding vegetation fires in Indonesia. First, we examined the trends in vegetation fires over the past decade, including the recent five years, analyzing whether fire activity has increased, decreased, or remained stable during this period. Next, we explored the extent to which fires intensify during El Niño years compared to non-El Niño years, given that El Niño events are typically associated with drier conditions. Additionally, we investigated whether satellite observations can effectively capture the increase in vegetation fires and the corresponding carbon monoxide (CO) emissions, which are critical indicators of fire intensity and air quality impacts. We assessed the magnitude of fire and fire intensity variations and CO enhancement during the typical dry season and compared these values to those observed during El Niño years. Further, we also analyzed the fire-CO emissions specific to peatlands. Our analysis provides valuable insights into the role of fires in driving CO pollution and air quality during El Niño and non-El Niño years in Indonesia.

2. Materials and Methods

2.1. Fire Data

We utilized the 375 m active fire product from the Visible Infrared Imaging Radiometer Suite (VIIRS), a key instrument onboard the Suomi National Polar-orbiting Partnership (Suomi NPP) and NOAA-20 satellites [36]. VIIRS is designed to capture high-resolution optical and thermal data, enabling near real-time detection of active fires worldwide. Operating across 22 spectral bands, including thermal infrared channels, the sensor allows for precise fire detection, even in remote or cloud-covered regions [37]. Compared to other coarser resolution satellite fire detection products like MODIS ($\geq$1 km), the enhanced 375 m resolution improves the detection of smaller fires and more accurate mapping of large fire perimeters. The VIIRS 375 m fire product builds upon the legacy of the MODIS fire product, utilizing a multi-spectral contextual algorithm to identify sub-pixel fire activity and other thermal anomalies in Level 1 (swath) input data [36]. This algorithm uses all five 375 m VIIRS channels to detect fires and distinguish land, water, and cloud pixels in the image [36]. Specifically, we used the VNP14IMG thermal anomalies product, which provides the fire location coordinates, detection time, fire radiative power (MW), brightness temperature of the I4 and I5 bands, and the confidence value of fire detection. The data is available in various formats, including TXT, SHP, KML, and WMS, making it easily integrable into geospatial analysis platforms. Although the VIIRS fire data is globally calibrated and validated, some biases can occur due to cloud cover, smoke, and atmospheric conditions that may obscure fire detection, leading to underreporting in certain areas. Temporal resolution limitations could also result in short-lived fires being missed. Despite these limitations, validation studies have shown that the VIIRS 375 m product detects over 80–90% of high-confidence fire pixels when compared to reference datasets or airborne fire observations [36]. Commission error rates are typically below 10% for high-confidence detections, and omission errors are significantly reduced compared to the coarser-resolution MODIS 1 km product. The product has also demonstrated robust detection capability for fires as small as 100–200 m in size under clear-sky conditions [36]. The latest VIIRS fire data can be accessed from the University of Maryland's fuoco SFTP server at sftp://fuoco.geog.umd.edu (accessed on 15 September 2025). For our analysis, we formatted the daily fire data into sequential monthly time-series inputs from 2012 to 2024 to capture temporal dependencies in fire occurrences. The initial product consisted of a shapefile containing a point feature for each detected fire; as such, any pixels that clouds had blocked were already excluded, and our calculations of fire radiative power included only confirmed fires (no erroneous sources such as sun glint or airglow). The full time span

of the data was used to assess trends in fire activity (see Sections 3.1 and 3.2); however, the air pollution data (see below) only covered 2019–2024 at the time of this project's beginning, and so was only compared to fire data from that period.

2.2. Air Pollution Data

To retrieve the Carbon Monoxide (CO) data corresponding to the VIIRS-derived vegetation fire data, we used the Tropospheric Monitoring Instrument (TROPOMI) aboard the Sentinel 5 Precursor [38]. TROPOMI is a spectrometer with ultraviolet, visible, and near- and shortwave infrared bands, which allow it to measure a variety of atmospheric components; the last of these, shortwave infrared (SWIR), is the most useful for the measurement of CO. Sentinel-5P, upon which TROPOMI is the sole payload, is a satellite created by the European Space Agency. From low Earth orbit, Sentinel-5P images the entire planet every 2 days. It is part of the "A-Train" constellation of Earth-observing satellites following the same orbit. Immediately ahead of Sentinel-5P in the "A-Train" is SUOMI-NPP, which passes over the same areas as Sentinel about five minutes beforehand. The CO images were captured by TROPOMI at a 7 km resolution [39]. While TROPOMI provides high-quality global CO measurements, retrieval accuracy can be influenced by factors such as cloud cover, surface reflectance, aerosols, and solar zenith angle. CO concentrations near the surface are also more difficult to detect due to limited vertical sensitivity in the lower troposphere. Validation studies indicate that TROPOMI CO data show a mean bias of less than ±6% compared to in situ surface and aircraft-based measurements, with correlation coefficients often exceeding 0.9 for background and urban conditions [39,40]. The total uncertainty in retrieved CO column densities is typically within 10% under clear-sky conditions and low aerosol loading. Overall, the dataset is well-suited for tracking large-scale pollution events such as biomass burning and has been successfully used in numerous regional and global fire emission studies. We used images from all months of 2019 through 2024 (the only years completely covered by existing data, at the time of this project's beginning), aggregated over monthly and/or yearly timescales for different facets of the analysis.

Further, we focused specifically on the forest fires and related CO emissions. We used MODIS land cover data (MCD12Q1) at https://modis.gsfc.nasa.gov/data/dataprod/mod12.php (accessed on 15 September 2025) to exclude all non-forest land cover types from the study area. The MODIS image for January 2019, the earliest within the period covered by the CO data, was used as a starting point. A forest mask was constructed based on the IGBP classification, retaining five forest-related classes: Evergreen Needleleaf, Evergreen Broadleaf, Deciduous Needleleaf, Deciduous Broadleaf, and Mixed Forest. All non-forest classes were excluded. We also sorted the fire and pollution data for peatlands, using a peatland geospatial layer obtained from the Global Forest Watch [41].

2.3. Data Processing

The following steps were followed for the data processing. The VIIRS active fire data F(x,y,t), originally at a spatial resolution of 375 m, was rescaled to a 10 km grid using a spatial averaging kernel K_{10km} as

$$F_{10km}(i,j,t) = \frac{1}{N}\sum_{x,y\in A_{ij}} F(x,y,t) \quad (1)$$

where $F_{10km}(i,j,t)$ is the monthly fire count per 10 km grid cells, N is the number of 375 m pixels in the 10 km cell, A_{ij} is the area of the (ij)-th grid cell. Similarly, the CO data from TROPOMI is averaged and aggregated to a similar resolution as,

$$C_{10km}(i,j,t) = \frac{1}{M}\sum_{x,y\in A_{ij}} C_{raw}(x,y,t) \quad (2)$$

where $C_{10km}(i,j,t)$ is the average CO column over the 10 km grid, $C_{raw}(x,y,t)$ is the original TROPOMI retrieval, M is the number of valid retrievals in cell (i,j). We then used the data specifically over the forest areas using MODIS land cover data as:

$$F_mask(i,j) = \begin{cases} 1, if L(i,j) \in ENF, EBF, DNF, DBF, MF, \\ 0, otherwise \end{cases} \quad (3)$$

where L(i,j) is the land cover type of the grid cell (i,j), ENF is the evergreen needle leaf forest; EBF is the Evergreen Broadleaf Forest, DNF is the Deciduous Needle Leaf Forest, DBF is the Deciduous Broadleaf Forest and MF is the Mixed Forest. In addition, we also evaluated fire-CO emissions over the peatlands as,

$$F_{10km}^{peat}(i,j,t) = F_{10km}(i,j,t) \cdot P(i,j) \quad (4)$$

$$C_{10km}^{peat}(i,j,t) = C_{10km}(i,j,t) \cdot P(i,j) \quad (5)$$

Here, P(i,j) = 1 if the grid cell is peatland, and 0 otherwise.

Using these data, the spatio-temporal correlations were addressed at 10 km grid cell intervals as,

$$\rho_{forest} = \text{corr}(F_{10km}(i,j,t) \cdot F(i,j),\ C_{10km}(i,j,t) \cdot F(i,j)) \quad (6)$$

$$\rho_{peat} = \text{corr}\left(F_{10km}^{peat}(i,j,t),\ C_{10km}^{peat}(i,j,t)\right) \quad (7)$$

To infer the temporal trends in the entire fire dataset (2012–2024), we used the Mann–Kendall seasonal trend test [42,43] including seasonal decomposition. It is a widely used non-parametric method for detecting monotonic trends in seasonal time series data. Unlike the traditional Mann–Kendall test, the seasonal version accounts for recurring seasonal patterns by analyzing each season (e.g., monthly fire data, in our case) separately before combining the results to determine an overall trend [44]. The test evaluates whether observations increase or decrease consistently over time within each season. Because it makes no assumptions about the data's distribution or linearity, it is particularly valuable where data often deviates from normality and displays seasonal cycles. The test outputs a test statistic (S), a normalized Z-score, and a significance level (p-value) indicating the presence and direction of a trend. We also applied the Seasonal Mann–Kendall test to detect trends in time series data while accounting for seasonality. In addition, the Theil–Sen slope estimator was used to calculate the median rate of change, providing a robust measure of trend magnitude, even in the presence of outliers. Also, seasonal decomposition was applied to the fire count time series data (2012–2024) of entire Indonesia to separate the data into different components which included trend, recurring seasonal variation, and residuals. The trend captures gradual increases or decreases in fire activity over time, while the seasonal component reflects systematic intra-annual patterns, such as peaks during specific months. The residuals represent unexplained variation after removing trend and seasonality, highlighting random fluctuations or potential anomalies. This decomposition allowed clearer interpretation of dominant fire patterns and facilitated the identification of unusual events beyond expected seasonal and trend behavior.

The flowchart for the methodology of data processing and analysis is given in Figure 2. The spatial analysis involved data processing in Google Earth Engine (GEE). The VIIRS derived monthly fire images were created by filtering the fire point features by date, then using GEE's reduceToImage method to turn the resulting monthly feature collection into an image; in the process, the count() reducer was applied to each 10 km pixel, so that its value would be the number of non-zero fire radiative power measurements included, i.e., the number of fires to occur in that pixel during that month and aggregated for a specific year. The corresponding twelve CO images for each year were averaged separately from

the twelve fire images, and the annual average fire image was added as an additional band to the annual average CO image.

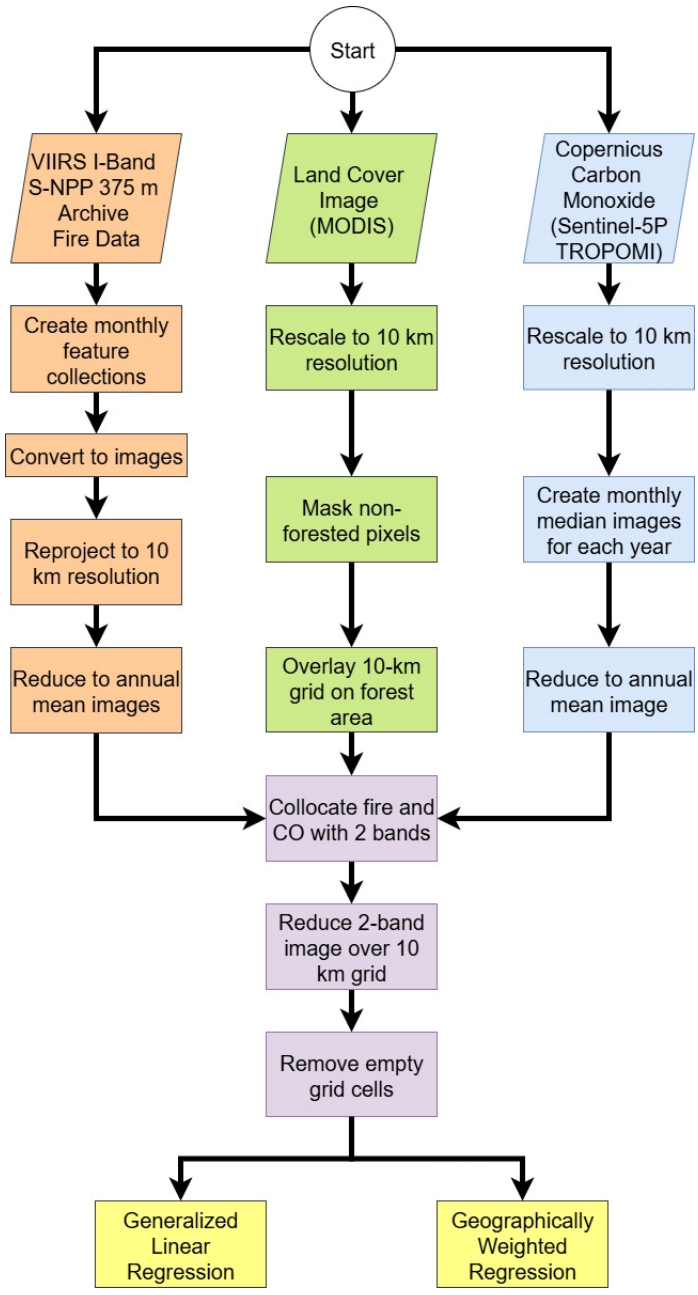

Figure 2. Methodology flowchart. Google Earth Engine (GEE) has been used for data processing.

A grid of 10 km cells was then overlaid upon the forest polygon, and the annual 2-band image was reduced over it, i.e., within each cell, the sum of all pixels was calculated and set as a new property of that cell. The resulting feature collection was further processed to remove empty grid cells and edges. The data was exported as shape files and then to spreadsheets for further statistical analysis. Our analysis represents only the pixels within forests. Thus, the data represent vegetation fires and corresponding CO analysis in those pixels. We also performed a temporal analysis, similarly to the spatial one, with the creation of monthly median carbon monoxide images. However, the fire data was not converted to an image this time. Instead, for each month, the total CO concentration and total FRP (the sum of all pixels) within the forest polygon and the total number of fire points that

intersected it were calculated, and these numbers were added to the polygon feature as additional properties. The data was then exported as a table for further statistical analysis.

2.4. Regression Analysis

To test the relationship between fires and CO, we used two different statistical methods, the traditional Linear Regression (LR) and Geographically Weighted Regression (GWR), to assess the relationship between fires and CO from 2019 to 2024.

Linear Regression (LR) is a fundamental statistical technique that models the relationship between a dependent variable and one or more independent variables by assuming a linear relationship. In its simplest form, the ordinary least squares (OLS) regression equation is expressed as

$$y = \beta_0 + \beta_1 x + \varepsilon \tag{8}$$

where y represents the dependent variable (CO concentration), x represents the independent variable (fire counts), β0 is the intercept, β1 is the regression coefficient indicating the strength and direction of the relationship, and ε is the error term accounting for unexplained variability. Traditional LR assumes spatial stationarity, meaning the relationship between fires and CO is constant across all locations. This assumption may not hold in spatially heterogeneous environments, where factors influencing fire and CO emissions vary regionally.

To address spatial variability, we used Geographically Weighted Regression (GWR), which extends LR by allowing regression coefficients to vary spatially. Unlike OLS, which estimates a single global relationship, GWR models local relationships at each spatial location. The GWR model is expressed as,

$$y_i = \beta_0(u_i, v_i) + \sum_{k=1}^{p} \beta_k(u_i, v_i) x_{ik} + \varepsilon_i \tag{9}$$

where (u_i,v_i) are the spatial coordinates of observation i, and β_k(u_i,v_i) are location-specific regression coefficients estimated separately for each spatial unit. The local coefficients are computed using a weighted least squares approach

$$\hat{\beta}(u_i, v_i) = \left(X^T W_i X\right)^{-1} X^T W_i Y \tag{10}$$

where X is the matrix of independent variables, Y is the vector of observed CO concentrations, and Wi is a spatial weighting matrix defining the influence of nearby observations. A kernel function determines the weights, commonly the Gaussian kernel:

$$w_{ij} = \exp\left(-\frac{d_{ij}^2}{2b^2}\right) \tag{11}$$

where d_{ij} is the Euclidean distance between locations *i* and *j*, and *b* is the bandwidth parameter controlling the spatial extent of the weighting function. The bandwidth is optimized using the Akaike Information Criterion (AIC) to balance model complexity and goodness-of-fit. The pseudo t-value for each variable was calculated by dividing β with the standard error to evaluate its relative importance in each 10 km grid; the variable with the largest pseudo t-value was deemed the dominant driver of fire. Using the chosen variables, GWR was performed annually from 2019 to 2024 using an adaptive kernel bandwidth, selected by minimizing the AICc. Overall, by incorporating spatial non-stationarity, GWR provides localized insights into the relationship between fires and CO, capturing regional variations that traditional linear regression may overlook. While LR offers a global perspective on the fire–CO relationship, GWR reveals spatially varying

trends, allowing for a more detailed understanding of how fire-induced CO emissions differ across regions through spatial maps.

3. Results

The total fire counts from 2012 to December 2024, covering the entirety of Indonesia, suggested an average of 21,271 fire counts per year. The monthly averages from January to December for the same corresponding period suggested the peak fire season as August, September, and October. Forests account for nearly 32.0% of total fires, and peatlands account for 21.9%. El Niño events can significantly impact different ecosystems in Indonesia, often leading to drier conditions and increased fire activity.

3.1. Trends in Vegetation Fires over the Past Decade

The trend in fire counts for the twelve years is given in Figure 3, wherein the enhancement in fires for El Niño years can be seen. Time series fire analysis from 2012 to 2024, monthly fires using the Mann–Kendall trend test, suggested a significant downward trend in fire activity. The null hypothesis (H_0: no trend) is tested against the two-sided alternative (H_1: there is a trend), and the results suggested a test statistic of −42, with an associated standard error (ASE) of 16.391, yielding a Z-value of −2.501 and a *p*-value of 0.012. Since the *p*-value is less than the commonly used significance level of 0.05, we rejected the null hypothesis and concluded that there is a statistically significant trend. The negative Z-value and Kendall Tau statistic of −0.538 indicated that the trend is downward, meaning fire activity has decreased over time. The Theil–Sen slope estimate further confirmed this decline, with a median slope of −502.154, suggesting a decrease of approximately 502 FC per month. The 95% confidence interval for the slope ranges from −1221.947 to −132.556, confirming that the trend is robustly negative.

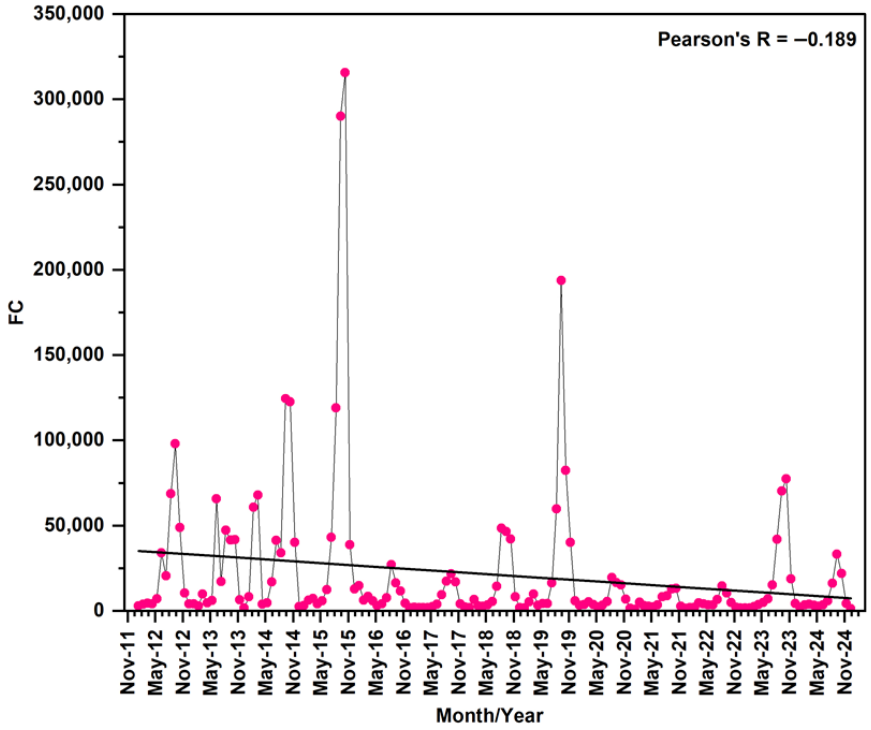

Figure 3. Fire counts (FC) in Indonesia, derived from VIIRS satellite data (2012–2024), show a clear declining trend over the years. The highest peaks correspond to increased fire activity during El Niño years.

In addition, the seasonal Kendall test also showed a significant and seasonally consistent decrease in the observed FC over time. The seasonal test evaluated the null hypothesis (H_0: no trend) against a two-sided alternative (H_1: there is a trend), while controlling for seasonality (e.g., monthly FC). The resulting test statistic was −344.000 with an associated standard error (ASE) of 56.780, resulting in a Z-value of −6.058 and a *p*-value of 0.000. The null hypothesis is rejected since the *p*-value is well below 0.05, indicating a significant trend exists even after accounting for seasonal variation. The negative Z-value and Kendall Tau statistic of −0.368 confirmed that the trend is downward, i.e., fire counts have decreased consistently over time across seasons in Indonesia. The Theil–Sen slope estimate was −376.583, suggesting a median decline of about 377 FC per month. The 95% confidence interval for the slope varied from −555.037 to −239.564, reinforcing the presence of a robust negative trend.

Figure 4 depicts the results from the seasonal decomposition of all VIIRS satellite-derived fire counts (top) and anomalies (bottom) between 2012 and 2024 across all of Indonesia. The top bar chart represents the percentage variation in fire counts by season across each month, with the y-axis showing the percentage contribution of the seasonal component to total variation in fire activity. At the same time, the x-axis represents months from January to December.

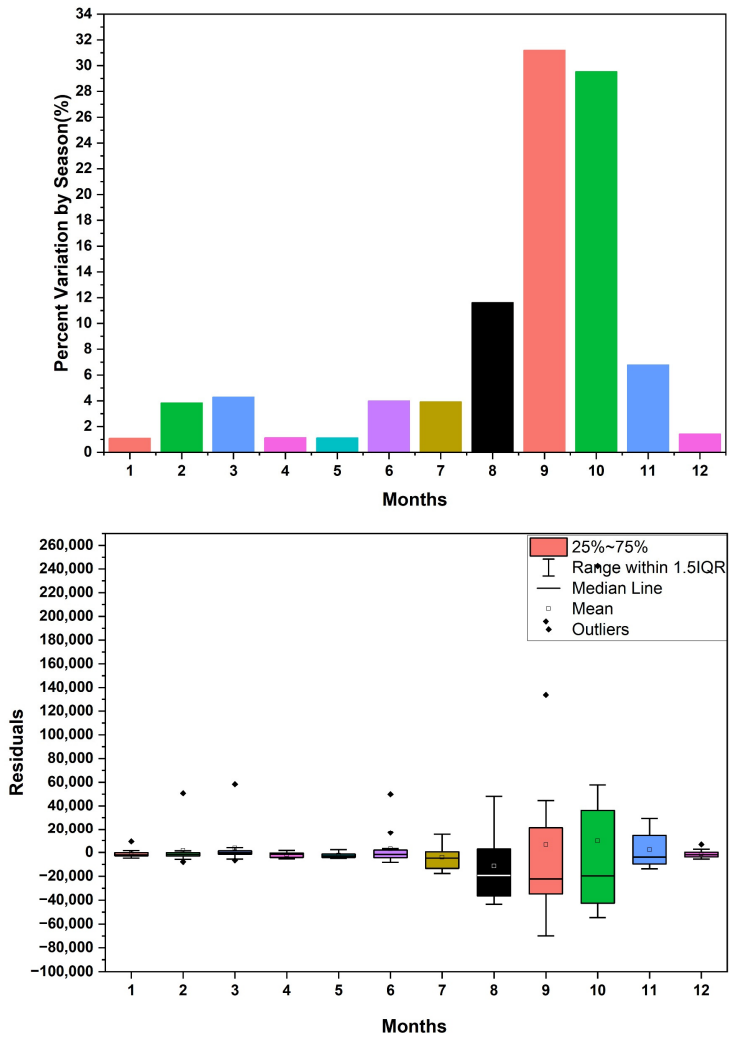

Figure 4. Seasonal decomposition of VIIRS satellite derived fire data (2012–2024). The top bar chart shows monthly percent seasonal variation in VIIRS-detected fire activity from 2012 to 2024, with peaks

during September and October, indicating a strong, recurring fire season. Other months show minimal seasonal influence, suggesting more irregular fire patterns. The bottom plot shows monthly box plots showing residuals in fire distribution from seasonal decomposition. The boxes represent the interquartile range (25–75%), with medians as horizontal lines and means as circles. Whiskers extend to 1.5×IQR, and dots indicate outliers. Variability is low from January to July and peaks from August to November, indicating a strong seasonal component.

The data reveal a strong seasonal pattern, with the highest variation occurring in September and October, each accounting for nearly 30% or more of the total seasonal variation. The seasonal decomposition suggests a well-defined peak fire season during the late monsoon to post-monsoon period. August also shows a moderate fire, contributing approximately 11%, indicating the onset of heightened fire activity during this time. In contrast, months from January through July and November and December show significantly lower seasonal fire contributions, typically below 6%, indicating that fire occurrences in these months are less frequent. The seasonal decomposition also highlights the predictability of fire activity in the late summer and fall months, reinforcing the seasonal nature of fire regimes in Indonesia during these 12 years. The bottom plot in Figure 4 shows monthly distributions of residuals derived from the seasonal decomposition of fire count time series (2012–2024). The boxes in the plot represent the interquartile range (IQR), capturing the middle 50% of anomaly values, with the horizontal line denoting the median. Whiskers extend to values within 1.5 × IQR, and data points beyond this threshold are shown as outliers. Small open circles mark the monthly means, enabling comparison with medians to assess skewness. The residuals from the seasonal decomposition represent the deviations of observed fire counts from the values expected after accounting for both the long-term trend and recurring seasonal patterns. Positive residuals indicate that fires were higher than expected in a given month, while negative residuals suggest they were lower. The box plots of residuals by month show how this unexplained variation is distributed. For most months, residuals are small and centered near zero, indicating that the decomposition captured the variation well. However, for peak fire months such as September and October, the residuals show a much wider spread, reflecting considerable variability likely driven by other factors such as drought conditions, climatic anomalies, or human activities. The dots outside the whiskers in the box plots represent unusually large deviations and can be interpreted as potential anomalies or extreme fire years.

3.2. Intensification of Fires During El Niño Years Compared to Non-El Niño Years

The fire activity and related CO emissions in Indonesia from December 2018 to December 2024, focusing on the influence of El Niño events, are shown in Figure 5a–d. The spatial variation in fires, including the CO during the El Niño year (2019) versus the non-El Niño year (2020), suggested a significant increase in fire hotspots all over Indonesia, covering Sumatra, Java, Bali, Kalimantan, Sulawesi, etc. The fire counts (FC) spiked dramatically during the El Niño periods, peaking at over 200,000 in mid-2019 and again reaching significant levels in 2023 (Figure 5a). Outside of these periods, fire counts remain relatively low and stable. Specifically, during the El Niño years, on average, fires were almost 533% more common during 2019 and 481% more common during the 2023 El Niño years, compared to non-El Niño years (2020, 2021, 2022). Similarly to FC, the Fire Radiative Power (FRP in megawatts), a measure of fire intensity, also surged sharply during the two El Niño phases, with a maximum in mid-2019, followed by a smaller peak in 2023, and remains subdued during non-El Niño months (Figure 5b).

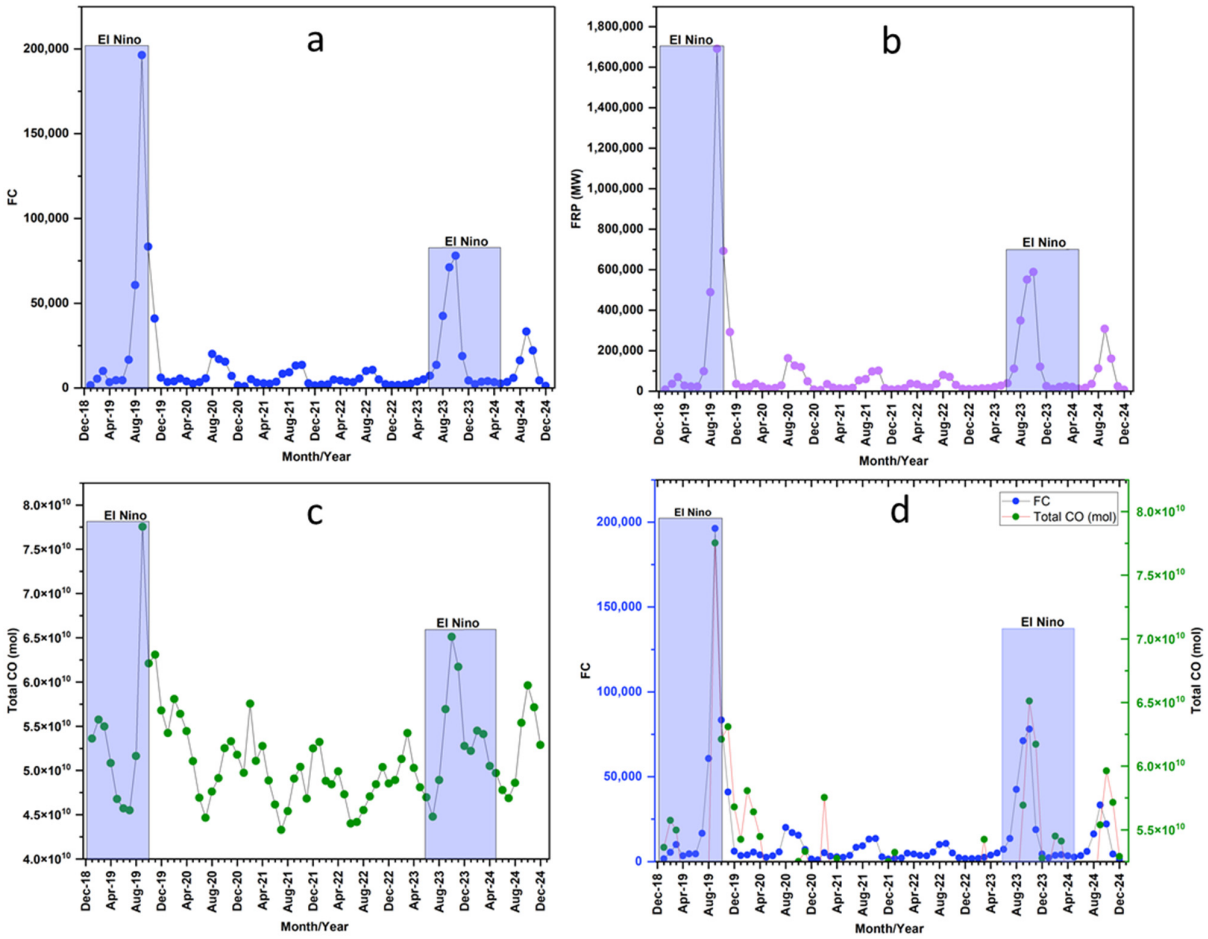

Figure 5. (**a**–**d**) Time-series plots depicting monthly fire counts (FC) (**a**), fire radiative power (FRP) (**b**), total CO emissions (**c**), and FC versus CO (**d**) for the entirety of Indonesia from 2018 to 2024. Peaks in fire activity align with El Niño events in 2019 and 2023 (shaded areas), highlighting their strong influence on fire activity and emissions.

The fire activity also strongly influences the total CO emissions in moles (Figure 5c). CO emissions peaked during the El Niño-induced fire periods, especially in 2019 when emissions exceeded 7.5×10^{10} mol, and increased again in 2023, though slightly less. The bottom right panel (Figure 5d) between FC and CO data on dual y-axes shows their temporal alignment, i.e., CO emissions closely follow spikes in FC, reaffirming the strong relationship between fires and atmospheric CO pollution. Shaded areas highlight the El Niño periods, underlining their role in amplifying fire occurrence, intensity, and emissions. In addition, analyzing all fire and CO data for the entire country, we also analyzed the data separately over forests (Figure 6a–d) and peatlands (Figure 7a–d). The results showed similar patterns with elevated FC, FRP, and CO during the El Niño events. However, peatlands showed relatively higher FC and CO emissions during the El Niño events. There is some overlap between the two areas, but neither completely contains the other; most Indonesian forests are not in peatlands, and the peatlands also include substantial areas of wetland.

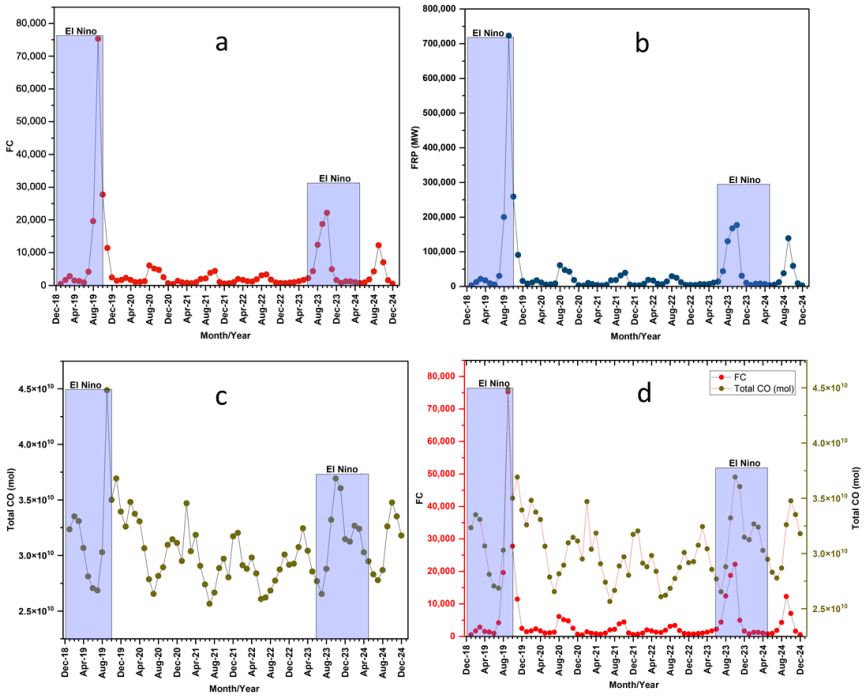

Figure 6. (**a**–**d**) Time-series plots depicting monthly fire counts (FC) (**a**), fire radiative power (FRP) (**b**), total CO emissions (**c**), and FC versus CO (**d**) for forested areas of Indonesia from 2018 to 2024. Peaks in fire activity align with El Niño events in 2019 and 2023 (shaded areas), highlighting their strong influence on fire activity and emissions.

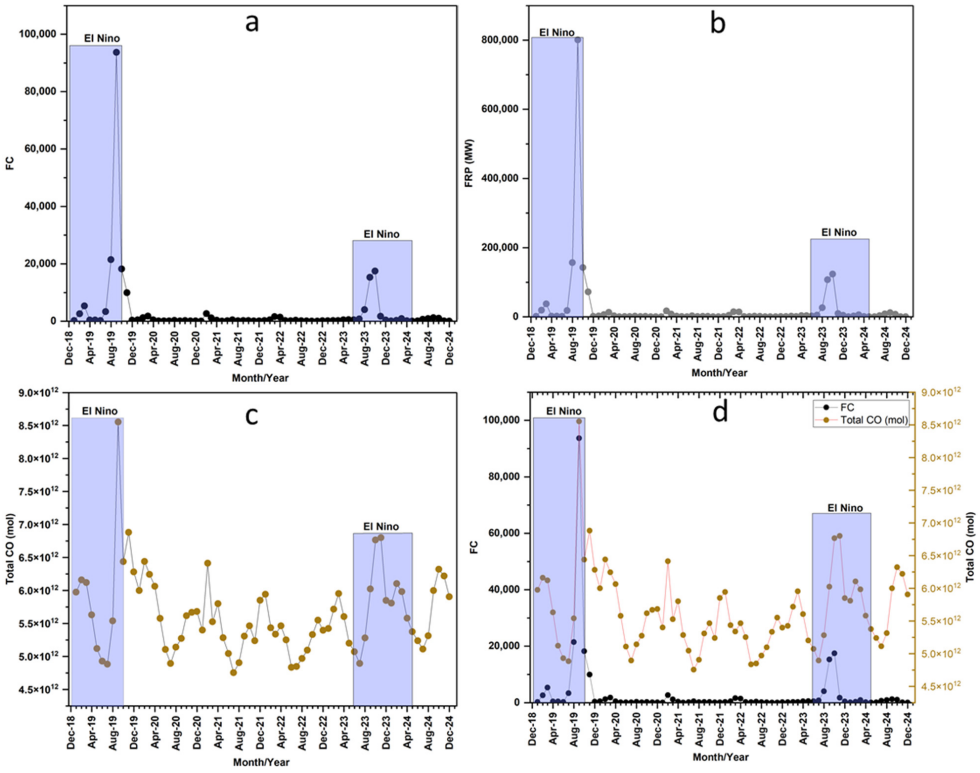

Figure 7. (**a**–**d**) Time-series plots depicting monthly fire counts (FC) (**a**), fire radiative power (FRP) (**b**), total CO emissions (**c**), and FC versus CO (**d**) for peatland areas of Indonesia from 2018 to 2024. Peaks in fire activity align with El Niño events in 2019 and 2023 (shaded areas), highlighting their strong influence on fire activity and emissions.

3.3. FC Versus CO and FRP Versus CO Emissions in Forests

The linear regression between the FC and CO in forested areas resulted in an R^2 of 0.37. Comparatively, the GWR results from August to October 2019–2024 suggested consistently strong model performance (Table 1; Figure 8). The R^2 values varied from 0.6979 in 2022 to 0.8306 in 2019, indicating that between 69.8% and 83.1% of the variance in CO concentrations was explained by fire activity. Adjusted R^2 values closely followed the R^2 values each year, varying from 0.6979 to 0.8301. This confirms that the model maintained appropriate complexity without overfitting while effectively capturing the spatial variability in the fire–CO relationship. AICc values were consistently very low (more negative), reflecting strong model parsimony and excellent fit. The lowest AICc value was recorded in 2020 at −120,965.45, suggesting that that year's model achieved the optimal balance between explanatory power and simplicity. Although a gradual increase in AICc was observed in 2022 and 2023, indicating slightly reduced model efficiency likely due to changes in fire patterns or CO emission behavior, the GWR models remained robust overall. A strong relation between FC and CO was observed in Central Kalimantan, Western Sulawesi, Southern Java, etc. (Figure 8).

Table 1. GWR results for fire count and CO relationships in forested lands of Indonesia. The Global R^2 describes what proportion of variation in CO concentration can be attributed to variation in fire count, when viewing both variables across the area as a whole.

GWR	2019	2020	2021	2022	2023	2024
Global R^2	0.8306	0.7666	0.7505	0.6979	0.7833	0.7077
AdjR^2	0.8301	0.7659	0.7498	0.6979	0.7827	0.7069
AICc	−110,908.1	−120,965.4	−120,758	−120,117.4	−115,355.2	−117,327.0

Compared to the GWR analysis of FC and CO, which showed strong and stable model performance from 2019 to 2024 with R^2 values ranging from 0.6979 to 0.8306, the FRP–CO relationship also demonstrated similarly high explanatory power, though with subtle differences in model behavior across years (Table 2). Both models revealed their highest R^2 in 2019 (0.8306 for FC–CO and 0.8305 for FRP–CO), confirming that fire activity, measured by frequency or intensity, had the strongest spatial correlation with CO concentrations during that year. However, while the FC–CO model maintained more consistent AICc values over time, the FRP–CO model showed a greater sensitivity in AICc, achieving the lowest value in 2020 (−120,931.50), suggesting a more efficient model fit in years with moderate fire intensity. From 2021 to 2022, both models experienced a decline in R^2 values, reflecting reduced fire activity and possibly greater spatial variability, but the FRP–CO model maintained slightly lower R^2 values in those years. In 2023, a resurgence in fire activity led to improved R^2 in both models (0.783 for FRP–CO vs. 0.7901 for FC–CO), with both continuing to show strong model performance. Overall, while both FC and FRP serve as strong predictors of CO variability, the FC–CO relationship produced slightly more stable fit metrics, whereas the FRP–CO relationship showed greater responsiveness to interannual changes in fire intensity and emissions structure. These complementary results highlight the value of using both fire frequency and intensity metrics to understand spatial patterns in atmospheric pollution from landscape fires.

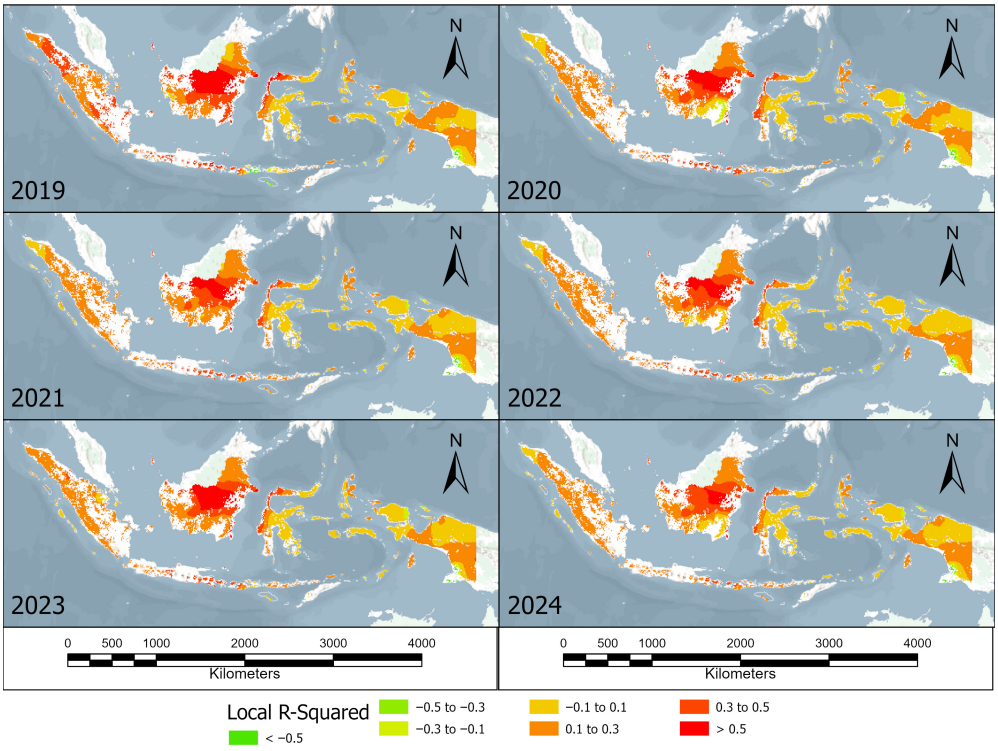

Figure 8. Fires and CO pollution in forested areas of Indonesia, based on Geographically Weighted Regression analysis for August–October during 2019–2024. The local R-squared value represents the proportion of variance in carbon monoxide explained by variations in fire counts at that particular location. In red areas, fires are the primary contributor to CO pollution, such as in central Kalimantan, western Sulawesi, and southern Java. In contrast, in green areas, fire counts have minimal influence on CO levels.

Table 2. GWR results for Fire Radiative Power (FRP) and CO relationships in forests of Indonesia. The Global R^2 describes what proportion of variation in CO concentration can be attributed to variation in FRP, when viewing both variables across the area as a whole.

GWR	2019	2020	2021	2022	2023	2024
Global R^2	0.8305	0.7659	0.7503	0.6965	0.783	0.7081
AdjR^2	0.8301	0.7652	0.7496	0.6956	0.7824	0.7073
AICc	−110,908	−120,931	−120,750	−120,062	−115,340	−117,342

3.4. FC Versus CO and FRP Versus CO Emissions in Peatlands

The GWR analysis evaluating the relationship between FC and CO concentrations in peatland areas from 2019 to 2024 revealed modest but consistent model performance (Table 3 and Figure 9). R^2 values varied from 0.1934 in 2024 to 0.2731 in 2019, indicating that fire activity explained 19.3% and 27.3% of the CO concentrations' variance over the study period. Adjusted R^2 values closely followed the R^2 trend, ranging from 0.1891 to 0.2698, confirming that the model retained a balanced complexity while avoiding overfitting. The AICc values remained consistently low (more negative) throughout the period, indicating strong model parsimony and a reliable fit. The lowest AICc value was observed in 2022 at −24,414.37, suggesting that that year's model achieved the most favorable balance between goodness-of-fit and simplicity. While R^2 values remained relatively modest compared to forest areas, and minor fluctuations occurred year to year, the consistently negative AICc values support the effectiveness of GWR in capturing the spatially variable relationship between fire activity and CO concentrations in peatland ecosystems.

Table 3. GWR results for fire counts and CO relationships in peatlands of Indonesia. The Global R^2 describes what proportion of variation in CO concentration can be attributed to variation in fire count, when viewing both variables across the area as a whole.

GWR	2019	2020	2021	2022	2023	2024
Global R^2	0.2731	0.2127	0.2103	0.1983	0.2044	0.1934
AdjR^2	0.2698	0.2085	0.2061	0.1939	0.2008	0.1891
AICc	−22,475.5	−23,909.1	−24,202.3	−24,414.4	−23,436.9	−23,736.8

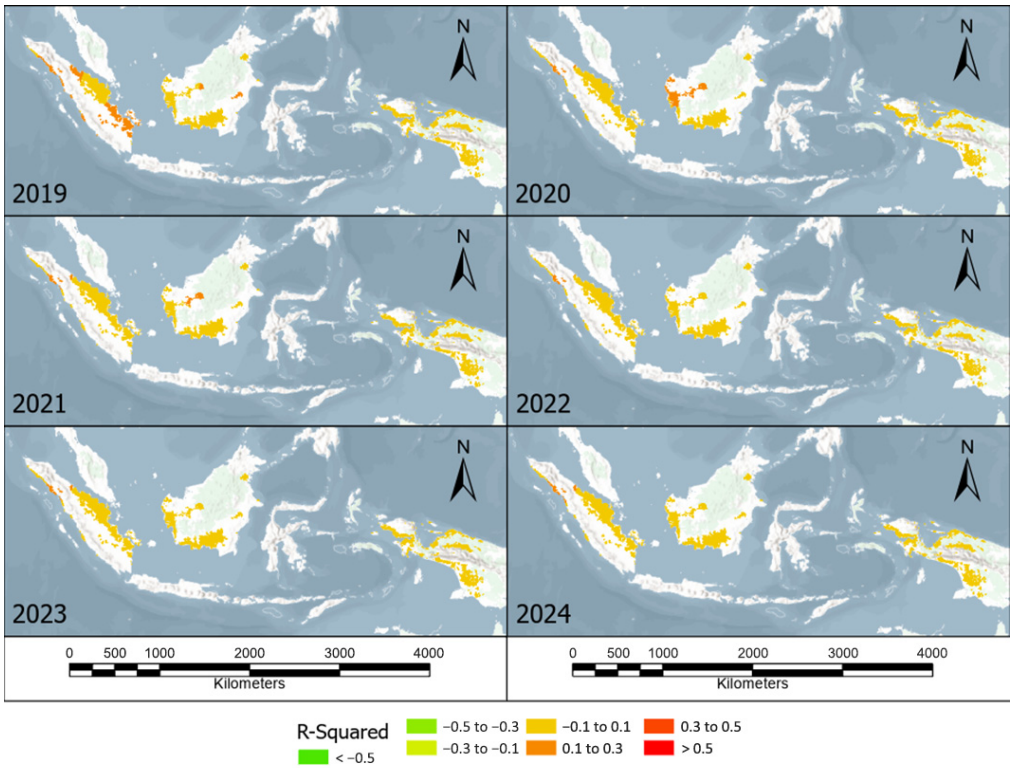

Figure 9. Geographically Weighted Regression (GWR) analysis of total fire counts and CO concentrations in the peatlands of Indonesia during August–October, 2019–2024. Local R-Squared values represent the proportion of variance in CO explained by fire counts at that particular location. Red areas indicate strong fire influence on CO pollution. Orange areas show minimal fire influence whereas green areas indicate no significant fire contribution to CO levels.

Compared to the GWR analysis of FC and CO concentrations in peatlands, which showed modest yet consistent explanatory power from 2019 to 2024 (R^2 ranging from 0.1934 to 0.2731; Table 4), the relationship between FRP and CO revealed slightly higher, but more variable, model performance. In both cases, the spatial relationship between FC and CO was notably weaker in peatlands than in forested areas, reflecting the unique combustion dynamics of peat soils. While the FC–CO model demonstrated stable R^2 values and persistently low AICc values across all years, indicating a reliable yet modest capacity to capture emission variability, the FRP–CO model showed slightly higher R^2 values overall (peaking at 0.3094 in 2019), suggesting a stronger but less stable connection between fire intensity and CO emissions. The FRP-based models also showed greater year-to-year fluctuations in AICc, indicating sensitivity to shifts in fire behavior and emission heterogeneity. Overall, while FRP offered a somewhat stronger predictor of CO concentrations than FC in peatlands, both metrics captured only a limited share of the spatial variability, underscoring the diffuse, smoldering nature of peatland fires and the challenges of modeling their emissions accurately.

Table 4. GWR results for fire radiative power (FRP) and CO relationships in peatlands of Indonesia. The Global R^2 describes what proportion of variation in CO concentration can be attributed to variation in FRP, when viewing both variables across the area as a whole.

GWR	2019	2020	2021	2022	2023	2024
Global R^2	0.3094	0.1926	0.1949	0.1851	0.2271	0.1972
AdjR^2	0.3063	0.1887	0.1908	0.181	0.2238	0.1935
AICc	−22,662.3	−23,819.7	−24,132.5	−24,357.2	−23,543.4	−23,757.2

3.5. Forest Fires and CO Pollution During El Niño Versus Non-El Niño Years

Fires in Indonesia are heavily influenced by El Niño events, which typically bring prolonged dry conditions that increase fire risks, particularly in fire-prone ecosystems such as forests and peatlands. The GWR results examining the relationship between fire occurrences and CO concentrations from 2019 to 2024 reflect this climatic influence in both the strength of the model's explanatory power (R^2) and its overall efficiency (AICc). In 2019, a residual influence from the weak-to-moderate El Niño that developed in late 2018 persisted into the year, contributing to drier-than-average conditions and heightened fire risks in parts of Indonesia. This is reflected in the GWR results, where the R^2 reached its highest value of 0.8306, indicating that over 83% of the variance in CO concentrations was explained by fire occurrences. The Adjusted R^2 closely followed at 0.8301, confirming strong model reliability. The AICc value, while not the lowest in the series, remained very low at −110,908.13, reflecting excellent model parsimony and fit during a year with widespread fire activity linked to lingering dry conditions.

In 2020–2022, fire activity reduced in intensity and spatial predictability following the absence of significant El Niño conditions and even brief La Niña phases. Correspondingly, the GWR model's explanatory power gradually declined, with R^2 values decreasing from 0.7666 in 2020 to 0.6979 in 2022. This decline likely reflects the more variable and less severe fire events during these wetter years, which reduced the strength of the spatial relationship between fires and CO concentrations. Notably, however, AICc values remained extremely low, with 2020 recording the lowest value of −120,965.45 across the entire study period, indicating the model maintained high efficiency and spatial sensitivity, even during years with relatively moderate fire activity.

In 2023–2024, the onset of a strong El Niño event in mid-2023, continuing into early 2024, created drier-than-normal conditions across much of Indonesia. This shift is mirrored in the GWR results, with R^2 values rising to 0.7833 in 2023, showing a resurgence in the strength of the fire–CO relationship as fire activity likely intensified under prolonged dry spells. The Adjusted R^2 remained high at 0.7827, and while the AICc increased slightly to −115,355.26 compared to earlier years, it still indicated an excellent model fit. In 2024, the R^2 decreased modestly to 0.7077, suggesting a slight reduction in fire intensity or spatial predictability of CO emissions as conditions possibly began to normalize towards the end of the El Niño event. However, the model retained its robustness with a strongly negative AICc of −117,327.00.

In summary, the GWR analysis captured the clear influence of El Niño-driven climate variability on fire activity and associated CO emissions in Indonesia. The model's highest explanatory power coincided with periods of El Niño-induced droughts in 2019 and 2023, while reductions in R^2 during intervening years reflect the dampening effect of wetter conditions and fewer severe fires. The consistently low AICc values across all years reinforce the strength and suitability of GWR in capturing the spatially heterogeneous relationship between fire counts and atmospheric CO concentrations in this dynamic, climate-sensitive region.

3.6. Peatland Fires and CO Pollution During El Niño Versus Non-El Niño Years

Peatland ecosystems in Indonesia are susceptible to climate variability, particularly during El Niño events, which lower water tables and significantly increase drier conditions, which favor fire susceptibility. The GWR results assessing the relationship between fire occurrences and carbon monoxide (CO) concentrations in peatlands from 2019 to 2024 reflect this climatic influence, though with a generally lower explanatory power than forested areas. In 2019, following a weak-to-moderate El Niño phase extending from late 2018 into early 2019, drier-than-normal conditions persisted in several peatland regions, increasing fire risks. The GWR model showed its highest explanatory power during this year, with an R^2 of 0.273, indicating that around 27.3% of the variation in CO concentrations was explained by fire occurrences in peatlands. The corresponding Adjusted R^2 of 0.2698 confirms the model's reliability and suitability during a year of elevated fire activity in these ecosystems. Between 2020 and 2022, the absence of strong El Niño conditions and episodes of La Niña and wetter weather likely suppressed fire activity in peatlands, contributing to a gradual decline in the model's explanatory power. R^2 values dropped from 0.2127 in 2020 to 0.1983 in 2022, reflecting reduced spatial predictability in the fire–CO relationship during these relatively wetter years. The Adjusted R^2 values followed a similar trend, declining from 0.2085 to 0.1939, suggesting that while fire events still contributed to CO variability, other factors such as decomposition emissions, small-scale fires, or peatland hydrology changes became more influential.

A strong El Niño onset in mid-2023, extending into early 2024, once again created drier conditions across Indonesia, including its extensive peatland regions. However, unlike in forests, the peatland fire–CO relationship exhibited a more muted response. R^2 values rose slightly from 0.1983 in 2022 to 0.2044 in 2023, suggesting a modest strengthening of the relationship as fire activity likely increased under dry conditions. Despite this, the R^2 did not reach 2019 levels, possibly due to localized fire management interventions, improved early warning systems, or shifts in land management practices. In 2024, R^2 declined further to 0.1934, indicating a slight reduction in the fire–CO relationship strength even as El Niño conditions persisted.

In summary, the GWR analysis highlights that while El Niño-induced droughts influence peatland fires, the spatial relationship between fire occurrences and CO emissions remains moderate, with R^2 values generally ranging between 19% and 27% over the study period. Peaks in explanatory power coincided with drier years such as 2019, while reduced values during wetter or more controlled years reflect the complex and localized nature of peatland fire dynamics. These results reinforce the importance of targeted fire monitoring and emission management in peatland regions, particularly under El Niño conditions when the risk of CO-emitting fires escalates.

4. Discussion

Our findings are consistent with those of similar studies in this region. In 2017, [45] reported that the intensity of Indonesia's fire season "is for a large part modulated by the El Niño–Southern Oscillation." Using the ATSR World Fire Atlas algorithm two and the Terra MODIS Thermal Anomalies/Fire product MOD14A1, [45] calculated total annual fire counts for 1997–2015. Their data indicate more than a 500% increase in fire counts during an average El Niño year (mean of 1997, 1998, 2002, 2006, 2009, 2014, and 2015) compared to an average non-El Niño year (mean of the remaining years in that period) [45]. This value closely aligns with our calculation of the same enhancement over a later time period. Also, other studies [46] showed that El Niño significantly increases the monthly number of fire hotspots in Kalimantan and Sumatra to more than twice the usual number in non-El Niño years. In the same study, it was noted that El Niño most strongly enhances fire activity

during the annual fire season, which is consistent with our observations. Similarly, it was found that, due to its influence on precipitation, El Niño exerts a substantial effect on fire activity in Borneo [47]. Additionally, like our present study, another study [48] linked El Niño–induced increases in fire activity to a corresponding rise in carbon emissions. A strong negative nonlinear relationship between precipitation and fire activity (R^2 ranging from 0.69 to 0.98, depending on the region and data source) was noted [28], which, like in [48], was attributed to drought periods associated with El Niño. A strong relationship between precipitation and visibility at regional airports, a proxy for smoke and air pollution from the fires, with R^2 values of 0.90 in Sumatra and 0.77 in Kalimantan was also reported in the same study [28].

Our analysis, utilizing remote sensing datasets, reveals critical insights into fire activity and emissions across Indonesia from 2012 to 2024, particularly in tropical forests and peatlands. Although Mann–Kendall tests confirm a significant downward trend in national fire counts, periodic intensifications during El Niño years highlight Indonesia's vulnerability to climatic extremes. Forests and peatlands, which accounted for 32.0% and 21.9% of total fires, respectively, are carbon-rich and ecologically fragile, necessitating strengthened mitigation and adaptation [19]. The forests and peatlands of Kalimantan, Sumatra, and Papua are among the world's most biodiverse and carbon-dense ecosystems [49]. Peatlands store disproportionately large carbon pools in organic soils and are particularly susceptible to degradation from drainage and fire, with disproportionate emissions during El Niño droughts [7,26].

The GWR results show CO emissions are strongly associated spatially with fire activity in forests and peatlands, with model performance peaking during the intense 2019 El Niño. The lower R^2 for peatlands suggests complex smoldering combustion, which satellite detection and modeling find challenging. Our findings highlight the need for targeted monitoring and fire suppression adapted to peatland biophysics.

Seasonal decomposition shows predictable fire peaks during dry months (August–October), offering a key window for preventive policies. Extreme fire events during El Niño years (2015–2016, 2019, 2023) indicate that policy improvements are still necessary to address climate extremes.

Fire counts and CO emissions surged over 500% during El Niño events, especially in Sumatra, Java, Bali, Kalimantan, and Sulawesi. Indonesia's multi-agency fire prevention frameworks involve inter-sectoral coordination, notably through the Peatland Restoration Agency (BRGM), which was effective and successfully restored approximately 1.6 million hectares of peatland and rehabilitated around 84,000 hectares of mangroves [50] but has now ceased operations. The National Disaster Management Authority (BNPB) also plays a key role [51,52]. BRGM aimed to restore over 2.5 million hectares of degraded peatlands via rewetting, revegetation, and livelihood revitalization.

Beyond environmental impacts, spikes in fire intensity and related CO emissions can pose serious public health risks, especially to vulnerable groups. CO from biomass burning impairs respiratory and cardiovascular health, necessitating coordinated air quality monitoring and public health advisories during fire seasons. Elevated emissions threaten Indonesia's FOLU Net Sink 2030 target to achieve a net carbon sink by 2030, which requires aggressive fire emission reductions [53].

Overall, Indonesia has made strides in landscape fire management with science-based strategies, including expanded peatland restoration led by BRGM in key fire-prone provinces. The ongoing community fire prevention programs empower villages with training and incentives for sustainable land use. Remote sensing agencies like BRIN and BMKG actively monitor fires, incorporating seasonal forecasts and El Niño outlooks into early warning systems. Further enhancements in early warning, health impact integration, and

enforcement of land clearing bans in agricultural frontiers are needed. Leveraging spatial remote sensing data can guide more targeted mitigation. With continued innovation and coordination, Indonesia is positioned to lead the region in fire mitigation and adaptation.

5. Conclusions

A detailed analysis of fire activity and associated carbon monoxide (CO) emissions across Indonesia from 2012 to 2024 revealed clear seasonal and interannual patterns strongly influenced by El Niño events. With an average of approximately 21,271 fire counts (FC) annually, peak fire activity consistently occurred between August and October, aligning with the dry and post-monsoon seasons. Forests and peatlands, accounting for 32.0% and 21.9% of all fires, respectively, were the most affected ecosystems, with substantial fire intensity and emissions spikes during major El Niño years. Our study provides robust empirical evidence that, although Indonesia has made progress in reducing fire activity over the past decade, significant fire-related emissions risks persist, particularly during El Niño years. Forests and peatlands remain high risk, high-impact fire zones. Strengthening mitigation and adaptation efforts in these ecosystems is essential not only for reducing national and regional carbon emissions but also for protecting public health and achieving long-term sustainability goals. A coordinated, science-informed, and climate-resilient fire management strategy, especially during El Niño evens, that emphasizes ecosystem restoration, community engagement, robust early warning systems, and real-time monitoring can greatly enhance Indonesia's ability to manage and mitigate future fire risks.

Author Contributions: Conceptualization, K.V.; methodology, G.M. and K.V.; software, K.V.; validation, G.M. and K.V.; formal analysis, G.M. and K.V.; investigation, G.M. and K.V.; resources, K.V.; data curation, G.M. and K.V.; writing—original draft preparation, G.M.; writing—review and editing, G.M. and K.V.; visualization, G.M. and K.V.; supervision, K.V.; project administration, K.V.; funding acquisition, K.V. All authors have read and agreed to the published version of the manuscript.

Funding: This research was funded by NASA Land Cover/Land Use Change Program, grant number SCEX2024D.

Data Availability Statement: Data will be made available on request.

Acknowledgments: Authors gratefully acknowledge the developers of the VIIRS and TROPOMI satellite products for providing the data.

Conflicts of Interest: The authors declare no conflicts of interest. The funders had no role in the design of the study; in the collection, analyses, or interpretation of data; in the writing of the manuscript; or in the decision to publish the results.

References

1. Goldammer, J.G. History of equatorial vegetation fires and fire research in Southeast Asia before the 1997–98 episode: A reconstruction of Creeping Environmental changes. *Mitig. Adapt. Strateg. Glob. Change* **2006**, *12*, 13–32. [CrossRef]
2. Vadrevu, K.P.; Lasko, K.; Giglio, L.; Schroeder, W.; Biswas, S.; Justice, C. Trends in vegetation fires in south and Southeast Asian countries. *Sci. Rep.* **2019**, *9*, 7422. [CrossRef] [PubMed]
3. Xu, C.; You, C. Agricultural expansion dominates rapid increases in cropland fires in Asia. *Environ. Int.* **2023**, *179*, 108189. [CrossRef] [PubMed]
4. Abdullah, A. *A Review and Analysis of Legal and Regulatory Aspects of Forest Fires in South East Asia*; WWF: Jakarta, Indonesia, 2002.
5. Miettinen, J.; Shi, C.; Liew, S.C. Influence of peatland and land cover distribution on fire regimes in Insular Southeast Asia. *Reg. Environ. Change* **2010**, *11*, 191–201. [CrossRef]
6. Li, P.; Feng, Z.; Jiang, L.; Liao, C.; Zhang, J. A review of swidden agriculture in Southeast Asia. *Remote Sens.* **2014**, *6*, 1654–1683. [CrossRef]
7. Page, S.E.; Siegert, F.; Rieley, J.O.; Boehm, H.-D.V.; Jaya, A.; Limin, S. The amount of carbon released from peat and forest fires in Indonesia during 1997. *Nature* **2002**, *420*, 61–65. [CrossRef]

8. Sun, J.; Liu, B.; Rustiami, H.; Xiao, H.; Shen, X.; Ma, K. Mapping Asia plants: Plant diversity and a checklist of vascular plants in Indonesia. *Plants* **2024**, *13*, 2281. [CrossRef]
9. Rahman, R.A.; White, B.; Ma, C. The effect of growth, deforestation, forest fires, and volcanoes on Indonesian Regional Air Quality. *J. Clean. Prod.* **2024**, *457*, 142311. [CrossRef]
10. Sarker, T.; Fan, P.; Messina, J.P.; Mujahid, N.; Aldrian, E.; Chen, J. Impact of urban built-up volume on urban environment: A case of Jakarta. *Sustain. Cities Soc.* **2024**, *105*, 105346. [CrossRef]
11. Hamdi, R.; Nugroho, H.D.; Setiawan, I.A. Long-term climate drivers of fire activity in Indonesia: A Mann-Kendall trend and correlation analysis. *Environ. Res. Lett.* **2025**, *20*, *in press*.
12. Irfan, M.; Koriyanti, E.; Saleh, K.; Hadi; Safrina, S.; Awaludin; Sulaiman, A.; Akhsan, H.; Suhadi; Suwignyo, R.A.; et al. Dynamics of Peatland Fires in South Sumatra in 2019: Role of Groundwater Levels. *Land* **2024**, *13*, 373. [CrossRef]
13. Goldstein, J.E.; Graham, L.; Ansori, S.; Vetrita, Y.; Thomas, A.; Applegate, G.; Vayda, A.P.; Saharjo, B.H.; Cochrane, M.A. Beyond slash-and-burn: The roles of human activities, altered hydrology and fuels in peat fires in central Kalimantan, Indonesia. *Singap. J. Trop. Geogr.* **2020**, *41*, 190–208. [CrossRef]
14. Suhardono, S.; Fitria, L.; Suryawan, I.W.; Septiariva, I.Y.; Mulyana, R.; Sari, M.M.; Ulhasanah, N.; Prayogo, W. Human activities and forest fires in Indonesia: An analysis of the Bromo incident and implications for conservation tourism. *Trees For. People* **2024**, *15*, 100509. [CrossRef]
15. Tacconi, L.; Muttaqin, M.Z. Reducing emissions from Land Use Change in Indonesia: An overview. *For. Policy Econ.* **2019**, *108*, 101979. [CrossRef]
16. Setiawan, A.M.; Lee, W.; Rhee, J. Spatio-temporal characteristics of Indonesian drought related to El Niño events and its predictability using the multi-model ensemble. *Int. J. Climatol.* **2017**, *37*, 4700–4719. [CrossRef]
17. Hayasaka, H. Fire weather conditions in plantation areas in northern Sumatra, Indonesia. *Atmosphere* **2023**, *14*, 1480. [CrossRef]
18. Hayasaka, H. Peatland Fire Weather Conditions in Sumatra, Indonesia. *Climate* **2023**, *11*, 92. [CrossRef]
19. Gaveau, D.L.; Salim, M.A.; Hergoualc'h, K.; Locatelli, B.; Sloan, S.; Wooster, M.; Marlier, M.E.; Molidena, E.; Yaen, H.; DeFries, R.; et al. Major atmospheric emissions from peat fires in Southeast Asia during non-drought years: Evidence from the 2013 sumatran fires. *Sci. Rep.* **2014**, *4*, 6112. [CrossRef] [PubMed]
20. Kiely, L.; Spracklen, D.V.; Wiedinmyer, C.; Conibear, L.; Reddington, C.L.; Archer-Nicholls, S.; Lowe, D.; Arnold, S.R.; Knote, C.; Khan, M.F.; et al. New estimate of particulate emissions from Indonesian peat fires in 2015. *Atmos. Chem. Phys.* **2019**, *19*, 11105–11121. [CrossRef]
21. Jim, C.Y. The forest fires in Indonesia 1997-98: Possible causes and pervasive consequences. *Geography* **1999**, *84*, 251–260. [CrossRef]
22. Kuwata, M. Atmospheric emissions, processes, and impacts of tropical peatland fire haze in Equatorial Asia: A Review. *Atmos. Environ.* **2024**, *331*, 120575. [CrossRef]
23. Zebua, N.; Ziraluo, Y.P.; Zebua, E.N. Environmental conservation in biology learning: An effort to increase students' awareness of environmental issues. *Int. J. Adv. Educ. Res.* **2025**, *1*, 145–156. [CrossRef]
24. Corning, S.N.; Boere, E.; Krasovskiy, A.; Lessa Derci Augustynczik, A.; Shepherd, T.; Ghosh, R.; Kraxner, F.; Havlík, P. Flammable futures—Storylines of climatic impacts on wildfire events and palm oil plantations in Indonesia. *Environ. Res. Lett.* **2024**, *19*, 114039. [CrossRef]
25. Sambodo, N.P.; Pradhan, M.; Sparrow, R.; van Doorslaer, E. When the smoke gets in your lungs: Short-term effects of Indonesia's 2015 forest fires on health care use. *Environ. Health* **2024**, *23*, 44. [CrossRef]
26. Turetsky, M.R.; Benscoter, B.; Page, S.; Rein, G.; van der Werf, G.R.; Watts, A. Global vulnerability of peatlands to fire and carbon loss. *Nat. Geosci.* **2015**, *8*, 11–14. [CrossRef]
27. Kiely, L.; Spracklen, D.V.; Wiedinmyer, C.; Conibear, L.; Reddington, C.L.; Arnold, S.R.; Knote, C.; Khan, M.F.; Latif, M.T.; Syaufina, L.; et al. Air quality and health impacts of vegetation and peat fires in Equatorial Asia during 2004–2015. *Environ. Res. Lett.* **2020**, *15*, 094054. [CrossRef]
28. Field, R.D.; van der Werf, G.R.; Fanin, T.; Fetzer, E.J.; Fuller, R.; Jethva, H.; Levy, R.; Livesey, N.J.; Luo, M.; Torres, O.; et al. Indonesian fire activity and smoke pollution in 2015 show persistent nonlinear sensitivity to El Niño-induced drought. *Proc. Natl. Acad. Sci. USA* **2016**, *113*, 9204–9209. [CrossRef] [PubMed]
29. Lohberger, S.; Stängel, M.; Atwood, E.C.; Siegert, F. Spatial evaluation of Indonesia's 2015 fire-affected area and estimated carbon emissions using Sentinel-1. *Glob. Change Biol.* **2018**, *24*, 644–654. [CrossRef] [PubMed]
30. Afira, N.; Wijayanto, A.W. Mono-temporal and multi-temporal approaches for burnt area detection using Sentinel-2 satellite imagery (a case study of Rokan Hilir Regency, Indonesia). *Ecol. Inform.* **2022**, *69*, 101677. [CrossRef]
31. Arjasakusuma, S.; Kusuma, S.S.; Vetrita, Y.; Prasasti, I.; Arief, R. Monthly burned-area mapping using multi-sensor integration of Sentinel-1 and Sentinel-2 and machine learning: Case study of 2019's fire events in South Sumatra province, Indonesia. *Remote Sens. Appl. Soc. Environ.* **2022**, *27*, 100790. [CrossRef]

32. Hanami, Z.A.; Amin, M.; Hustim, M.; Putri, R.M.; Torabi, S.E.; Ramadhani, A.A.T.; Suryati, I. Spatial–Temporal Changes in Air Pollutants in Four Provinces of Sumatra Island, Indonesia: Insights from Sentinel-5P Satellite Imagery. *Urban Sci.* **2025**, *9*, 42. [CrossRef]
33. Wati, T.; Panjaitan, A. Forest fires detection in Indonesia using satellite Himawari-8 (case study: Sumatera and Kalimantan on august-october 2015). *IOP Conf. Ser. Earth Environ. Sci.* **2017**, *54*, 012053. [CrossRef]
34. Sofan, P.; Yulianto, F.; Sakti, A.D. Characteristics of false-positive active fires for biomass burning monitoring in Indonesia from VIIRS data and local geo-features. *ISPRS Int. J. Geo-Inf.* **2022**, *11*, 601. [CrossRef]
35. Elvidge, C.D.; Zhizhin, M.; Baugh, K.; Hsu, F.C. Identification of smoldering peatland fires in Indonesia via triple-phase temperature analysis of VIIRS nighttime data. In *Biomass Burning in South and Southeast Asia*; CRC Press: Boca Raton, FL, USA, 2021; pp. 25–38.
36. Schroeder, W.; Oliva, P.; Giglio, L.; Csiszar, I.A. The new VIIRS 375 M active fire detection data product: Algorithm description and initial assessment. *Remote Sens. Environ.* **2014**, *143*, 85–96. [CrossRef]
37. Justice, C.O.; Román, M.O.; Csiszar, I.; Vermote, E.F.; Wolfe, R.E.; Hook, S.J.; Friedl, M.; Wang, Z.; Schaaf, C.B.; Miura, T.; et al. Land and cryosphere products from Suomi NPP VIIRS: Overview and status. *J. Geophys. Res. Atmos.* **2013**, *118*, 9753–9765. [CrossRef] [PubMed]
38. Veefkind, J.P.; Aben, I.; McMullan, K.; Förster, H.; de Vries, J.; Otter, G.; Claas, J.; Eskes, H.J.; de Haan, J.F.; Kleipool, Q.; et al. Tropomi on the ESA sentinel-5 precursor: A GMES mission for global observations of the atmospheric composition for climate, air quality and ozone layer applications. *Remote Sens. Environ.* **2012**, *120*, 70–83. [CrossRef]
39. Borsdorff, T.; Aan de Brugh, J.; Hu, H.; Aben, I.; Hasekamp, O.; Landgraf, J. Measuring carbon monoxide with tropomi: First results and a comparison with ECMWF-IFS Analysis Data. *Geophys. Res. Lett.* **2018**, *45*, 2826–2832. [CrossRef]
40. Sha, M.K.; Langerock, B.; Blavier, J.-F.L.; Blumenstock, T.; Borsdorff, T.; Buschmann, M.; Dehn, A.; De Maziere, M.; Deutscher, N.M.; Feist, D.G.; et al. Validation of methane and carbon monoxide from Sentinel-5 Precursor using TCCON and NDACC-IRWG stations. *Atmos. Meas. Tech. Discuss.* **2021**, *14*, 6249–6304. [CrossRef]
41. Global Peatlands. Available online: https://data.globalforestwatch.org/datasets/gfw::global-peatlands/about (accessed on 1 July 2025).
42. Mann, H.B. Nonparametric tests against trend. *Econometrica* **1945**, *13*, 245–259. [CrossRef]
43. Kendall, M.G. *Rank Correlation Methods*, 4th ed.; Griffin: London, UK, 1975.
44. Hirsch, R.M.; Slack, J.R.; Smith, R.A. Techniques of trend analysis for monthly water quality data. *Water Resour. Res.* **1982**, *18*, 107–121. [CrossRef]
45. Fanin, T.; van der Werf, G.R. Precipitation–fire linkages in Indonesia (1997–2015). *Biogeosciences* **2017**, *14*, 3995–4008. [CrossRef]
46. Nurdiati, S.; Sopaheluwakan, A.; Septiawan, P. Spatial and temporal analysis of El Niño impact on land and forest fire in Kalimantan and Sumatra. *Agromet* **2021**, *35*, 1–10. [CrossRef]
47. Wooster, M.J.; Perry, G.L.; Zoumas, A. Fire, drought and El Niño relationships on Borneo (Southeast Asia) in the pre-MODIS ERA (1980–2000). *Biogeosciences* **2012**, *9*, 317–340. [CrossRef]
48. Pan, X.; Chin, M.; Ichoku, C.M.; Field, R.D. Connecting Indonesian fires and drought with the type of El Niño and phase of the Indian Ocean Dipole during 1979–2016. *J. Geophys. Res. Atmos.* **2018**, *123*, 7974–7988. [CrossRef]
49. Miettinen, J.; Shi, C.; Liew, S.C. Land cover distribution in the peatlands of Peninsular Malaysia, Sumatra and Borneo in 2015 with changes since 1990. *Glob. Ecol. Conserv.* **2016**, *6*, 67–78. [CrossRef]
50. BRGM Dissolved After Nine Years of Service: Over 1.6 Million Hectares of Peatland and Mangroves Restored. Available online: https://tanahair.net/brgm-dissolved-after-nine-years-of-service-over-1-6-million-hectares-of-peatland-and-mangroves-restored/ (accessed on 1 July 2025).
51. Wicaksono, A. Peatlands restoration policies in Indonesia: Success or failure? *IOP Conf. Ser. Earth Environ. Sci.* **2022**, *995*, 012068. [CrossRef]
52. Djuyandi, Y.; Casnoto, H.; Hidayat, W. Military operations other than war (MOOTW): Synergy of Indonesian National Armed Forces (TNI) and National Disaster Management Agency (BNPB) in Disaster Management. *Humanit. Soc. Sci. Rev.* **2019**, *7*, 111–121. [CrossRef]
53. Husain, R.; Korbaffo, J. Indonesia's FOLU Net Sink 2030 strategy: Assessing progress and policy gaps. *Environ. Policy Gov.* **2024**, *34*, 45–62. [CrossRef]